Journal of Magnetism and Magnetic Materials 497 (2020) 166066

Contents lists available at ScienceDirect

Journal of Magnetism and Magnetic Materials

journal homepage: www.elsevier.com/locate/jmmm

Generation of complex magnetic phase diagram of single crystalline $Sm_{0.50}Ca_{0.25}Sr_{0.25}MnO_3$ compound using magnetocaloric effect

Dipak Mazumdar[a,*], Kalipada Das[b], Susmita Roy[a], I. Das[a]

[a] CMP Division, Saha Institute of Nuclear Physics, HBNI, 1/AF, Bidhannagar, Kolkata 700064, India
[b] Department of Physics, Seth Anandram Jaipuria College, 10 Raja Naba Krishna Street, Kolkata 700005, India

A B S T R A C T

A detail study has been performed for the $Sm_{0.50}Ca_{0.25}Sr_{0.25}MnO_3$ compound in its single crystalline form. Distinctly different nature in their magnetocaloric responses (with temperature and external magnetic field variation) were found depending upon the direction of the external magnetic field. Additionally, we have constructed magnetic phase diagram from the magnetic and magnetocaloric effect. Different features in magnetic phase diagram were addressed considering the shape induced magnetic moments configuration in different orientation.

1. Introduction

Magnetocaloric effect (MCE) gets an utmost importance in the front line research regarding the demand of environment friendly cooling technology at the present time [1–10]. MCE is the measure of isothermal magnetic entropy change (ΔS) or adiabatic temperature change (ΔT) of any magnetic materials in the presence of external magnetic field [11,12]. For any magnetic materials, variation of the magnetic entropy change is very much influenced at the vicinity of the disorder-order (paramagnetic-ferromagnetic) transition. In general, with decreasing temperature from its paramagnetic(PM) (magnetic disorder) state it shows a long range magnetic ordering (ferromagnetic) below transition temperature [13–15]. From the isothermal magnetization data, variation of the temperature dependent of magnetic entropy change (ΔS) can be calculate by using Maxwell's thermodynamic relation (MR) [16] which is given below

$$\Delta S = \int_0^H (\partial M/\partial T) dH \quad (1)$$

The situation become quietly different for the existence of the strong irreversibility in magnetization [17–19]. Such ambiguity can be conquered by the appropriate correction as indicated by Paramanik et al. for the polycrystalline Dy_5Pd_2 compound to construct the magnetic phase diagram from the magnetocaloric effect [20]. In case of the doped perovskite manganites, generally correlated nature of the magnetic and magneto-transport properties are found [21–23]. In many situations, MCE study was used as a powerful tool to understanding the complicated electrical transport and magneto-transport properties of several materials having different types of the magnetic transition [24–27]. Generally, for the second order phase transition (SOPT), MR was used frequently to calculate the magnetic entropy change. However, for the materials having first order magnetic phase transition (FOPT), the magnetocaloric effect were reported earlier [28–33]. In several cases, large MCE were reported using Maxwell's relation (MR) [30–32]. Regarding this context many authors have disputed about the numerical values of MCE determined using MR [29,34–36]. Moreover for the samples having large hysteresis and FOPT, MCE calculation using Clausius-Clapeyron equation (CC) also reported [37–39]. Considering above all the facts recently Kataoka et. al. and Flores et al. reported their results about the applicability of MR in case of materials having FOPT [40,41].

Among the perovskite manganite materials except $La_{1-x}Ca_xMnO_3$ and $La_{1-x}Sr_xMnO_3$, the most well studied compound is $Sm_{1-x}B_xMnO_3$ (B = Ca, Sr). Due to its fascinating transport, magneto-transport and magnetic properties with different values of 'x' and choice of bivalent elements (B), this compound attracts a substantial attention to the on going research in this field [42–45]. During last few years, Sm-Ca-MnO_3 system was widely studied in their polycrystalline as well as nanocrystalline forms [44,46]. However, comparatively a less effort was paid to study the physical properties in the single crystalline form of the compound. To explore the underlying physical origin of several properties as well as for technological point of view, single crystalline forms of compound is much more superior compared to polycrystalline sample [47–49]. A numerous physical properties were greatly modified due to the distinct grain boundaries effect. Whereas, in single crystal forms, compound exhibits much more smooth intrinsic response [50–54].

Apart from external magnetic field, magnetic and magneto-

* Corresponding author.
E-mail address: dipak.mazumdar@saha.ac.in (D. Mazumdar).

https://doi.org/10.1016/j.jmmm.2019.166066
Received 13 September 2019; Received in revised form 19 October 2019; Accepted 26 October 2019
Available online 31 October 2019
0304-8853/

transport properties of spontaneously phase separated doped manganite are greatly defer with temperature as propagation of nucleated ferromagnetic patches take place with temperature variation [55]. According to the reported studies on $Sm_{0.5}Ca_{0.5}MnO_3$ compound, the charge ordering transition is near to 250 K and it shows robust charge ordered state in nature [56,57]. At T = 4.2 K, the required magnetic field is H ~ 600 kOe to melt this charge ordering [58]. As $Sm_{0.5}Sr_{0.5}MnO_3$ is a disordered ferromagnetic (FM) compound at low temperature [59,60], so by doping of Sr-ions in the place of Ca-ions, charge ordering become weaken and critical melting field also reduced and extreme value of magnetoresistance was achieved. Very recently Banik et al. had reported a novel route to destabilize the charge ordered phase by partial doping of Ca-site by Sr-ion having larger ionic radius [61]. In their study it was reported that charge ordered state of polycrystalline $Sm_{0.5}Ca_{0.25}Sr_{0.25}MnO_3$ (SCSMO) compound is melted in presence of H ~ 48 kOe external magnetic field at T = 2 K, resulting a huge magnetoresistance ~10^{15}% for this optimal doped compound [61]. The modification of the ground state with external magnetic field as well as doping also analyzed through the Monte Carlo simulation [61]. However, the general effect of the grain boundaries on the physical properties can not be neglected in case of the polycrystalline compound [61]. Moreover, due to the reduction of grain boundary effect, filed induced meta-magnetic transition may be expected at lower field values. Considering those mentioned context, we have prepared the single crystalline $Sm_{0.5}Ca_{0.25}Sr_{0.25}MnO_3$ (SCSMO) compound and studied its magnetic and magnetocaloric properties in detail.

For any magnetic materials, the magnetic phase diagram plays an important role to elucidate the nature of magnetic ground state of a compound[62–66]. The general techniques used to generate magnetic phase diagram are neutron diffraction, magnetization etc. The neutron diffraction is much more involved measurement technique, which requires much bigger infrastructure in comparison with the others. For that reason, the study of magnetization is generally used to generate the magnetic phase diagram due to its simplicity in measurement technique. There also an alternative way to deduce the magnetic phase diagram namely magnetocaloric effect (MCE). Very few authors have used this efficient method to generate magnetic phase diagram [67–69]. Another important point is that, due to the absorption of neutrons in normal Gd and Sm-based compounds, it is very difficult to use this technique (neutron diffraction) to generate magnetic phase diagram for such compounds. Considering those facts MCE technique was utilized to generate the magnetic phase diagram of Sm-based single crystalline like our SCSMO compound. Regarding the context of the necessity of generation of magnetic phase diagram, it is worth mentioning that the ground state of the SCSMO compound was markedly modified with the external magnetic field as described by Banik et al. earlier [61]. Henceforth, to fully make clear the ground state modifications via external magnetic field, we have constructed the magnetic phase diagram of the single crystalline SCSMO compound.

Our experimental results suggest that the charge ordered state in the single crystalline compound becomes more weaken compared to its polycrystalline form. Additionally, the constructed magnetic phase diagram explains the modification of the ground state depending upon the direction of the external applied magnetic field. Regarding the issue of construction of phase diagram, it is worth mentioning that the critical parameters were deduced from temperature and field dependence of magnetization (M(T) and M(H)) and magnetic entropy change (ΔS (T)) data. For magnetic entropy change calculation, MR was utilized in this study as there is no role of the magnitude of the magnetocaloric entropy change.

2. Experimental details

The polycrystalline SCSMO compound was prepared by conventional solid-state reaction method by using high purity Sm_2O_3 (99.99%), $CaCO_3$ (99.95%), $SrCO_3$ (99.995%) and MnO_2 (99.9%) powders. Before use, Sm_2O_3 was preheated at 800 °C for overnight. Well-mixed powder of all the above mentioned raw materials in a stoichiometric ratio was heated at 900 °C for 48 h.with intermediate grindings. The polycrystalline SCSMO compound was then reground and pressed into seed and feed rods of 6 mm in diameter under hydrostatic pressure. Finally, the rods were sintered at 1300 °C for 72 h. in air. The single crystals of SCSMO were grown in a four-mirror image furnace (Crystal System Co.) with the help of traveling solvent floating zone technique in the atmosphere of oxygen to avoid oxygen deficiency. During the growth process, the feed and seed rods were rotated at a speed of 25 rpm in opposite directions and the growth rate was maintained at 3.0 mm/h.

For basic characterization, X-ray diffraction study at room temperature was performed using Rigaku TTRAX-III diffractometer with Cu-K_α source. Profile fitting, using Rietveld refinement technique indicates the single phase nature of the compound. Magnetic measurements were performed by utilizing a super conducting quantum interference device (SQUID) (Quantum Design) in the temperature range 2–380 K and magnetic field up to 70 kOe. The magnetic properties of the compound were measured along two different orientations of the sample with respect to magnetic field direction which were noted in this manuscript as H∥ G.D. and H⊥ G.D. (G.D. represents growth direction of the single crystal). Regarding this context, information about the G. D. is very important. Recently, Radheep et al. had reported the detailed characterization of $Sm_{0.55}(Sr_{0.5}Ca_{0.5})_{0.45}MnO_3$ compound in its single crystalline form (very close to our studied SCSMO compound) and pointed out that G. D. as the C-axis [70]. Additionally the extracted lattice parameters are almost identical with our present studied system. Hence it may be argued that the G. D. is along the C-axis in the present case also.

3. Results and discussion

3.1. X-ray diffraction

The Rietveld refinement (profile fitting) technique was used for the structural analysis of as cast powdered SCSMO single crystal with Fullprof software. The room temperature X-ray diffraction pattern along with the profile fitting data is shown in Fig. 1. Our study indicates the chemically single-phase nature of the compound, yielding an orthorhombic crystal structure with the Pnma space group. No impurity peak has been observed over the whole range of diffraction pattern. The unit cell parameters determined from the profile fitting analysis are a = 5.421(5) Å, b = 5.412(5) Å, and c = 7.569(4) Å which gives a unit cell volume of 222.154(5) $Å^3$.

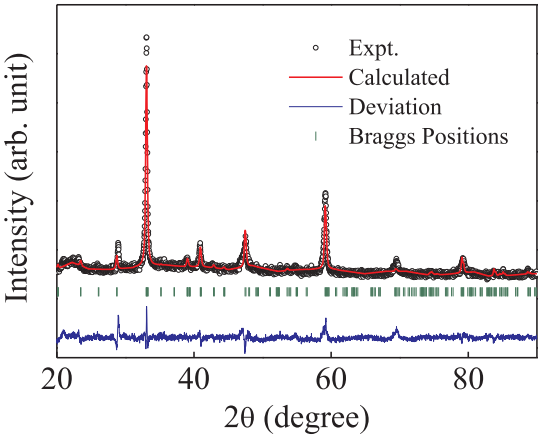

Fig. 1. Room temperature X-ray diffraction pattern along with the profile fitting data for powdered single crystalline $Sm_{0.5}Ca_{0.25}Sr_{0.25}MnO_3$ compound.

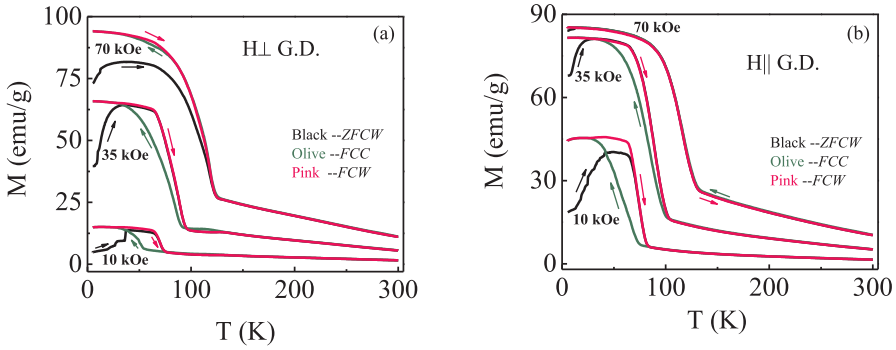

Fig. 2. Temperature dependence of Magnetization measured at 10 kOe, 35 kOe and 70 kOe magnetic fields in ZFCW, FCC and FCW protocols for single crystalline $Sm_{0.5}Ca_{0.25}Sr_{0.25}MnO_3$ compound. Magnetization was measured when magnetic field was applied perpendicular to the growth axis of the crystal ((a) H⊥ G.D.) and also along the growth axis direction ((b) H|| G.D.) of the sample. The black curve represents the ZFCW data, Olive curve represents the FCC data and pink curve represent the FCW data. The arrow marks are for the guidance of the observer.

3.2. Magnetic properties

To explore the magnetic ground state of the single crystalline compound, magnetization (M) as a function of the temperature (M-T) in the presence of different external magnetic fields have been carried out. M-T data were recorded in three different protocols namely zero field cooled warming (ZFCW), field cooled cooling (FCC), and field cooled warming (FCW).

Temperature dependence of magnetization (M-T) for three different applied magnetic fields along both the directions viz H⊥ G.D. and H|| G.D. of the single crystal have been shown in Fig. 2. At low fields, there is a hump observed at $T < 50$ K in the ZFCW magnetization data which may be the spin-blocking temperature. This spin-blocking temperature started to shift toward lower temperatures with increasing applied magnetic fields and it started to disappear at high magnetic fields. A strong irreversibility can be seen in between FCC and FCW magnetization curves at low fields (10 kOe and 35 kOe), which is nothing but the signature of the coexistence of different magnetic phases and this phase coexistence is suppressed with further increase of applied magnetic field. This strong irreversibility present in the sample may be linked to the presence of large magnetostriction[19]. One can clearly see that the magnetization increases very quickly upon application of 10 kOe magnetic field along H|| G.D. orientation as compared to H⊥ G.D. orientation. This may be because the easy axis of the single crystalline compound lies along the growth axis of the compound. Now, to further investigate the ground state of the system in presence of external perturbation i.e magnetic field in our case, we have been measured M-T by three different protocols along both the directions of the sample as shown in Figs. 3 and 4. From these M-T data, the noticeable antiferromagnetic (AFM) transition appears at $T \sim 150$ K in ZFCW, FCC and FCW protocols (Fig. 3)). With further lowering the temperature, compound goes to a ferromagnetic (FM) state at $T \sim 100$ K. The shifting of the transition temperature towards higher value appeared with the application of different magnetic fields. Such nature has been reported earlier in different compounds [20]. Regarding this context, it is worth noting, the existence of spin blocking in the ZFCW data even in single crystalline sample. In addition to that, even in presence of very small magnetic field, the ferromagnetic nature of the sample exists at low temperature. Hence it may be argued, the spin blocking in ZFCW magnetization is associated with the breaking of the collinear arrangement of magnetic moments at the interface of ferromagnetic and AFM unit cells. In contrast to that different nature in magnetization was found when magnetic field was applied along the growth axis of the sample. In this case the AFM signature was hidden at high temperature. However, the decreasing nature in magnetization was found at lower temperature in ZFCW protocol similar as cross-sectional (H⊥ G.D.) magnetization measurement.

For deeper understanding about the low temperature ground state, the magnetization as a function of magnetic field (M-H) have been carried out in both orientations of the sample with respect to magnetic field. The measured M-H data at $T = 2$ K is shown in Fig. 5. In case of H⊥ G.D. (Fig. 5(a)), magnetization increases linearly with magnetic field up to 25 kOe, response as AFM nature of the ground state. Above 25 kOe magnetic field, meta-magnetic transition takes place and magnetization rapidly increases with the magnetic field and reach the saturation. However, the isothermal magnetization measured along H|| G.D. direction exhibits distinct behavior compared to the H⊥ G.D. measurement. Along H|| G.D. magnetization, at very lower value of magnetic field, ferromagnetic like nature was initiated. But the value of the magnetization is very small compared to the saturation value. The saturation magnetization appears followed by two step like meta-magnetic transitions. First meta-magnetic transition take place at

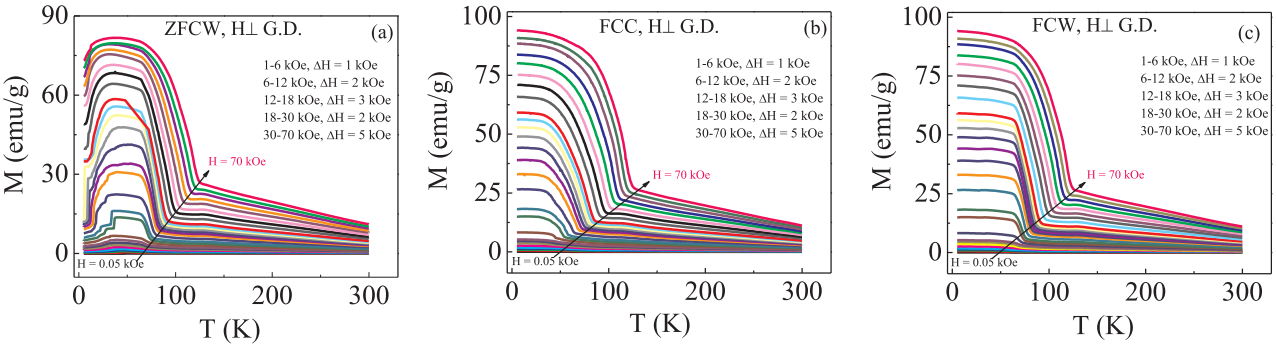

Fig. 3. Magnetization as a function of temperature at different external magnetic field in ZFCW, FCC and FCW protocols for single crystalline $Sm_{0.5}Ca_{0.25}Sr_{0.25}MnO_3$ compound. Magnetization was measured when magnetic field was applied perpendicular to the growth axis (H⊥ G.D.) of the sample.

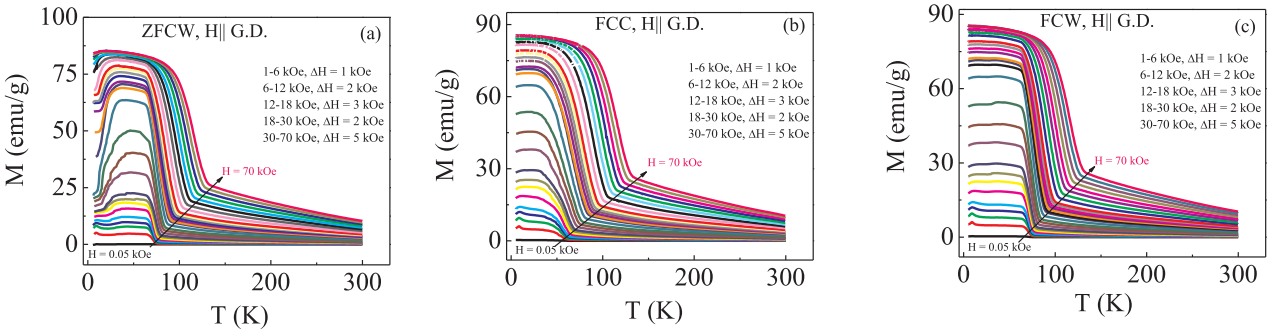

Fig. 4. Magnetization as a function of temperature at different external magnetic field in ZFCW, FCC and FCW protocols for single crystalline $Sm_{0.5}Ca_{0.25}Sr_{0.25}MnO_3$ compounds. Magnetization was measured when magnetic field was applied along the growth axis (H|| G.D.) of the sample.

H = 27 kOe. Whereas, second transition appears at H = 45 kOe. After subsequent field cycling, the sample reveals soft ferromagnetic nature implying the irreversible transition between the charge-ordered and FM state pointing towards the reduction of the canting angle of the AFM phase with increment of magnetic fields. It has been reported previously by Dho et.al that this kind of irreversible nature of magnetization is observed in Pr-based manganites [71]. According to their study, the spin moments of Mn ions are pinned by the magnetically ordered Pr-moments and block their moments in the saturated region which is responsible for this irreversible nature. In our case, Sm ion may play the same role, but the meta-magnetic steps observed in this compound may not be influenced by the magnetic nature of the A-site cations [72]. This occurrence of meta-magnetic steps may be explained by the scenario of the martensitic-like transition [73,74].

Both temperature and magnetic field dependent magnetization study for the single crystalline SCSMO sample indicates that the ground state nature is quietly different depending upon the direction of the applied magnetic field. To summarize the above mentioned experimental results, a decreasing nature in magnetization was found in ZFCW protocols for both cases (shown in Fig. 3 and Fig. 4)). In addition to that, after meta-magnetic transition along H⊥ G.D. direction, magnetization increases almost linearly having different slope before saturation. However, magnetization measured along H|| G.D. direction exhibits two sharp transition at H = 27 and 45 kOe magnetic fields.

3.3. Magnetocaloric effect

To visualize the complicated nature of the magnetic ground state, study of MCE has drawn considerable attention. We have calculated the change of magnetic entropy along both the orientations of the sample under application of various magnetic field. The MCE effect was calculated from the temperature dependent magnetization (measured in different protocols) by employing Maxwell's thermodynamic relation as given Eq. (1). Calculated magnetocaloric entropy change with temperature at different external magnetic field along both the orientations have been shown in Fig. 6. In addition to a very bare signature of AFM transition at T ~ 150 K (Fig. 6(a)), a pronounced ferromagnetic transition was found at T ~ 75 K in all protocols. Below 50 K, no transition signature appears in FCC and FCW protocols. However, in ZFCW protocol, magnetocaloric entropy change, − ΔS alter its sign i.e. inverse magnetocaloric effect (IMCE) has been observed and with lowering the temperature it goes towards zero, like an AFM signature. Qualitatively similar nature also present in calculated − ΔS(T) data along H|| G.D. direction of the sample (Fig. 6(b)) except the high temperature AFM phase.

As reported earlier, it is clear that in the presence of the external magnetic field, FM transition temperature shifts towards high temperature and AFM transition temperature shifts towards lower temperature region [16]. However, in our studied sample due to the predominant effect of the competing FM phases, the AFM like transition at low temperature is almost inert irrespective of the magnetic field. To avoid such ambiguities, the varying base field technique is more appropriate as described by Paramanik et al. [16]. Additionally, for magnetic phase diagram construction, extraction of the critical parameters by using this method is the most accurate technique [16]. Considering this point, we have calculated magnetocaloric entropy change for magnetic field change of 5 kOe from its initial field value along both the orientation of the compound only for ZFCW protocol. From Fig. 7(a) and (b), it is clearly visible that with increasing magnetic field value, AFM transition at low temperature shifts toward further lower temperature region. In addition to that the FM transition temperature in both cases moves towards higher temperature regime with increasing magnetic fields.

We have calculated the associated change of heat capacity (ΔC_P

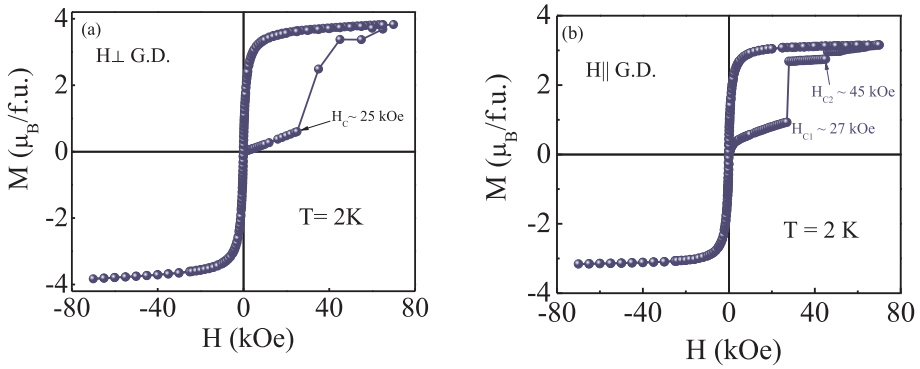

Fig. 5. Magnetization as a function of external magnetic field at T = 2 K for single crystalline $Sm_{0.5}Ca_{0.25}Sr_{0.25}MnO_3$ compounds. (a) Magnetization was measured when magnetic field was applied perpendicular to the growth axis (H⊥ G.D.) of the sample, and (b) Magnetization was measured when magnetic field was applied along the growth axis (H|| G.D.) of the sample.

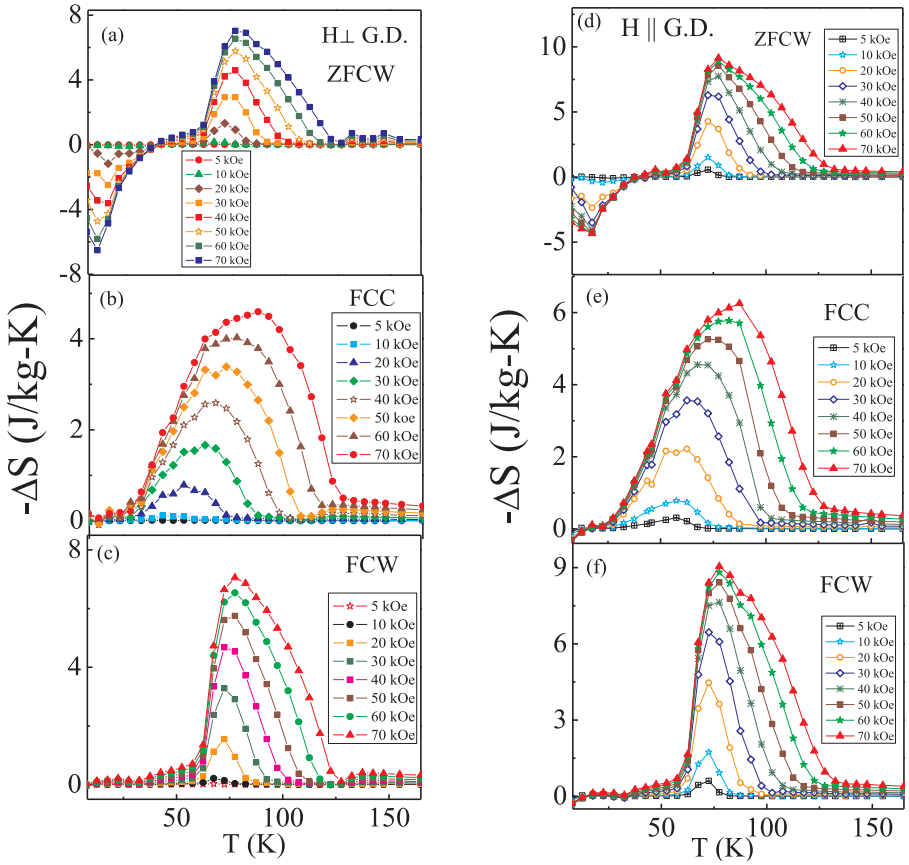

Fig. 6. Magnetocaloric entropy change as a function of temperature at different external magnetic fields in three different protocols viz. ZFCW, FCC and FCW for single crystalline $Sm_{0.5}Ca_{0.25}Sr_{0.25}MnO_3$ compound. (a) Magnetization was measured when magnetic field was applied perpendicular to the growth axis (H⊥ G.D.) of the sample, and (b) Magnetization was measured when magnetic field was applied along the growth axis (H‖ G.D.) of the sample.

(T,H)) in the presence of different magnetic fields to discriminate the influence of the magnetic phase transitions as observed in the variation of magntocaloric entropy change data. The change of heat capacity (ΔC_P (T,H)) associated with a magnetic field variation from 0 to H is calculated by using the following relation as described in earlier study [75].

$$\Delta C_P(T, H) = C_P(T, H) - C_P(T, 0) \quad (2)$$

$$= T\frac{\delta(\Delta S(T, H))}{\delta T}$$

The changes of heat capacity calculated from magnetic entropy changes ΔS vs T data, where the base field was taken as zero, are plotted as a function of temperature only for ZFCW protocol both for H⊥ G.D. and H‖ G.D. direction of the sample which is shown in Fig. 8. It is clearly seen that ΔC_P (T,H) shows a crossover from negative ($T < T_C$) to positive ($T > T_C$) values around T_C due to the magnetic phase transition accompanied by an increase in the ΔC_P (T,H) values with the applied magnetic fields associated with it. Such nature of ΔC_P (T,H) was also reported previously by Nassri et al. [76]. It can be seen from the figures that T_C started shifting towards higher temperature with increasing applied magnetic field, which is nothing but a FM-PM or AFM like magnetic phase transition (FM). But in case of H⊥ G.D. direction, above T_C, the ΔC_P (T,H) undergoes a sudden change from positive to negative, reflects the short-range AFM-PM like magnetic phase transition (AFM-I) similar to the M-T as well as − ΔS vs T plots (Fig. 3 and 6(a)). Regarding this context it is worth mentioning that this

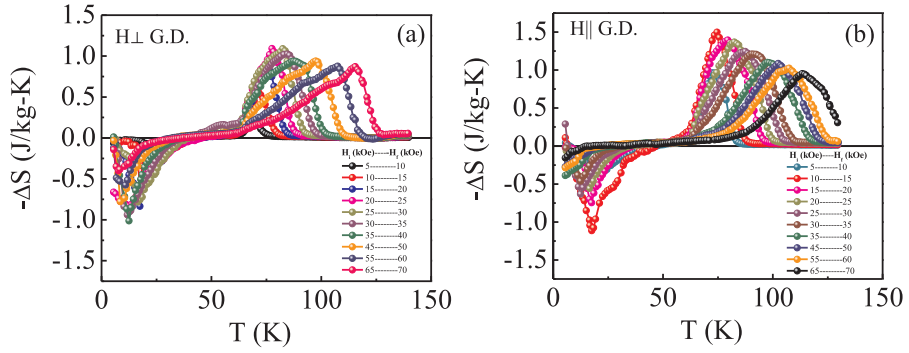

Fig. 7. Isothermal magnetic entropy change for consecutive field values (interval 5 kOe) (− ΔS) as a function of temperature for single crystalline $Sm_{0.5}Ca_{0.25}Sr_{0.25}MnO_3$ compound. (a) Magnetization was measured when magnetic field was applied perpendicular to the growth axis (H⊥ G.D.) of the sample, and (b) Magnetization was measured when magnetic field was applied along the growth axis (H‖ G.D.) of the sample.

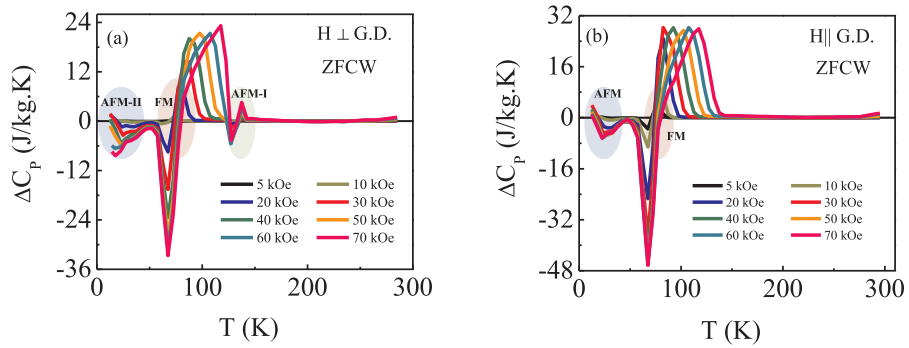

Fig. 8. Changes of heat capacity in the presence of different magnetic fields, calculated from the magnetocaloric entropy changes in both orientation of the sample in ZFCW magnetization measurement protocol. The different magnetic phase transitions are marked by shaded regions in top panels of the figures.

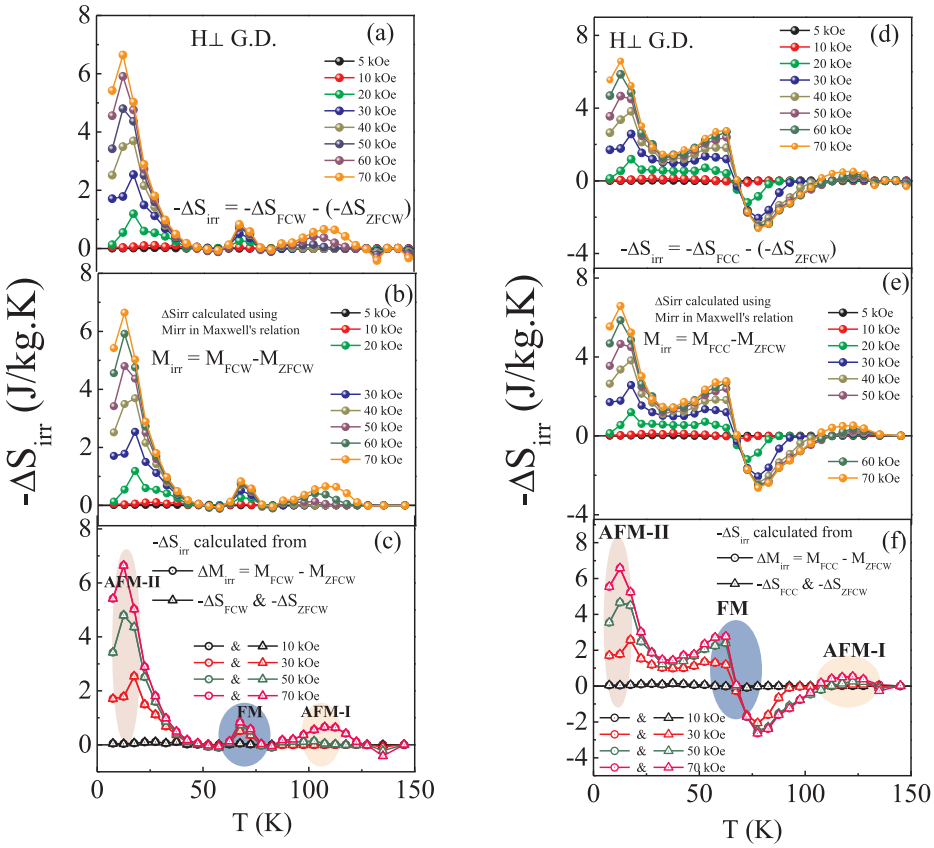

Fig. 9. Irreversible entropy changes calculated both from taking difference between FC entropy change and ZFCW entropy change (a and d) and considering the irreversible magnetization (M_{FCC}-M_{ZFCW} and M_{FCW}-M_{ZFCW}) (b and e) in Maxwell's equation (Eq. (1)). The irreversible entropy change, calculated in both ways give similar results (c and f) for single crystalline $Sm_{0.5}Ca_{0.25}Sr_{0.25}MnO_3$ compound when magnetic field was applied perpendicular to the growth axis (H⊥ G.D.) of the sample. The different magnetic phase transitions are marked by shaded regions in the lower panels of the figures.

characteristics (high temperature AFM-I -PM transition) is absent along growth axis (H⊥ G.D.) of the sample. Similarly, the presence of low temperature FM-AFM like magnetic phase transition (AFM-II for H⊥ G.D. and AFM for H|| G.D. as indicated in Fig. 8)) can be noticed along both the axes of the sample.

Another meaningful technique to detect the feeble magnetic transitions is the plotting irreversible order parameter magnetization (measured in different protocols)[20]. Regarding this framework, it should also be mentioned that, as the magnetocaloric entropy change is related with the first order derivative of magnetization, hence transitions should be more pronounced in calculated $-\Delta S_{irr}(T)$ data [20]. So, first we have calculated the irreversible magnetization, (M_{irr}) from the difference of magnetizations of FC and ZFC [19] and calculated $-\Delta S_{irr}(T)$ in both cases by using Maxwell's equation of entropy (Eq. (1)). Alternatively, we have also calculated $-\Delta S_{irr}$ from the difference of $-\Delta S_{FC}$ and $-\Delta S_{ZFC}$. The calculated value of $-\Delta S_{irr}$ (T) in both procedures exhibits good agrement to each other which is shown clearly in the lower panel of Fig. 9 and 10. Different magnetic transitions associated with the sample have been represented by the shaded areas in the lower panels of Figs. 9 and 10. As one can clearly see from Fig. 9(c) and (f), in the temperature range of 100 K–125 K, a peak has appeared due to the presence of short-range AFM ordering (AFM-I) along cross-sectional orientation (H⊥ G.D.) of the sample. This transition is further followed by a FM like transition with further lowering the temperature. Signature of low temperature AFM ordering (AFM-II) due to the presence of robust charge-ordered state can be clearly seen. Moreover, there is no

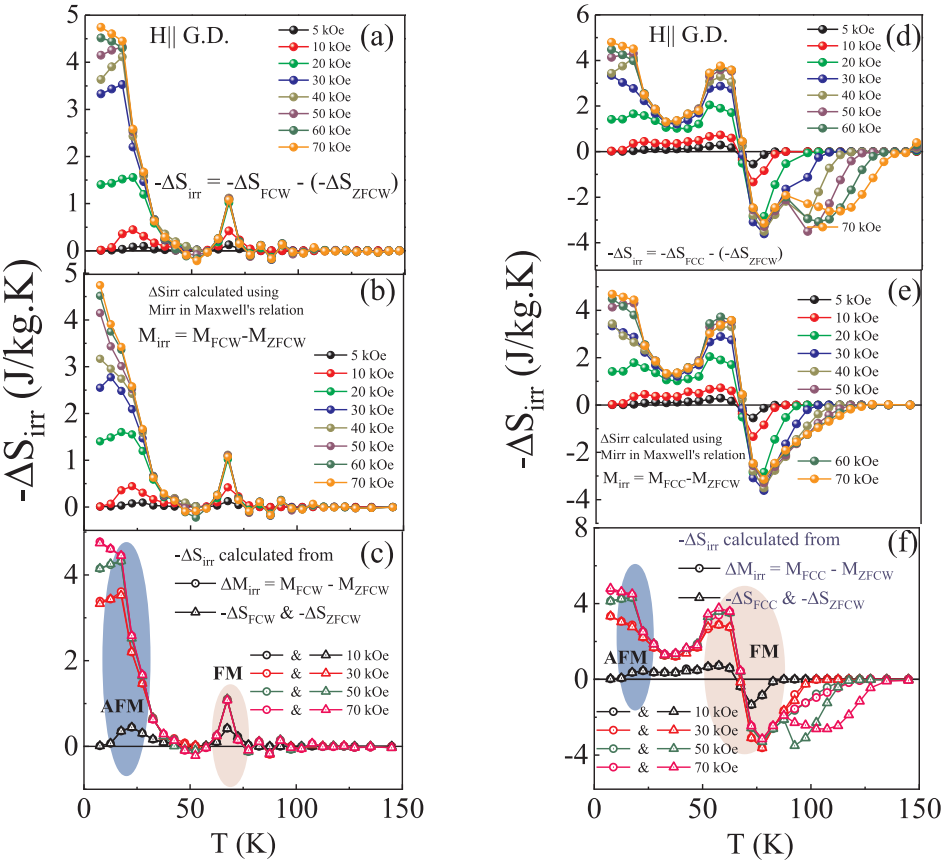

Fig. 10. Irreversible entropy changes calculated both from taking difference between FC entropy change and ZFCW entropy change (a and d) and considering the irreversible magnetization (M_{FCC}-M_{ZFCW} and M_{FCW}-M_{ZFCW}) (b and e) in Maxwell's equation (Eq. (1)). The irreversible entropy change, calculated in both ways give similar results (c and f) for single crystalline $Sm_{0.5}Ca_{0.25}Sr_{0.25}MnO_3$ compound when magnetic field was applied along the growth direction (H|| G.D.) of the sample. The different magnetic phase transitions are marked by shaded regions in the lower panels of the figures.

signature of any high temperature AFM like ordering (AFM-I) along the growth axis (H|| G.D.) of the sample which is also absent in $-\Delta S_{irr}$ (T) plots as shown in the lower panel of Fig. 10(c) and (f). This AFM-II ordering may causes the strong irreversibility in between the FCC and FCW data as clearly seen in M-T data of Fig. 2 and which may be responsible for the inverse nagnetocaloric effect (IMCE) at the low temperature regime of ZFCW data.

The presence of these different kind of magnetic phases as discussed in the above paragraph in case of single crystalline SCSMO along both the orientations have also been found in different analysis like both temperature and magnetic field dependence of magnetization (M-T and M-H), magnetocaloric effect (ΔS vs T), changes of heat capacity (ΔC_P (T,H)), and irreversible magnetocaloric effect ($-\Delta S_{irr}$ (T)) which were discussed earlier in this text.

3.4. Magnetic phase diagram

As far as the experiments were concerned, almost identical critical parameters (transition fields and transition temperatures) were extracted from different experimental protocols. From the extracted critical temperature and corresponding critical magnetic field values from M-T, M(H), and MCE ($-\Delta S(T)$), we have constructed magnetic phase diagram of the single crystalline $Sm_{0.50}Ca_{0.25}Sr_{0.25}MnO_3$ compound in different geometry (viz. H⊥ G.D. direction and H|| G.D. orientations) as shown in Fig. 11. The extracted critical parameters (transition temperatures and critical magnetic fields) from all the measurements followed the identical phase boundaries. From the constructed magnetic phase diagram, it can be noticed that the PM to AFM phase boundary (AFM-I) is almost inert with the application of the magnetic field along H⊥ G.D. orientation of the compound (Fig. 11(a)). However, due to further lowering of temperature, FM transition temperature shifts toward higher temperature. Similarly, at very low temperature (T < 50 K), another AFM phase boundary (AFM-II) appears and it is shifted towards low temperature region with increasing magnetic field. On the other hand, when magnetic field is applied along the growth axis (H|| G.D.), FM and low temperature AFM phase boundaries exhibits almost same nature as H⊥ G.D. orientation. However, unlike H⊥ G.D. H⊥ G.D. direction, inert PM to AFM phase boundary at high temperature region is absent. This indicates the presence of strong anisotropy along two different directions of the single crystal.

4. Summary

To summarize, details magnetic and magnetocaloric effect of single crystalline compound of $Sm_{0.5}Ca_{0.25}Sr_{0.25}MnO_3$ have been presented. Our experimental results indicate distinct magnetic and magnetocaloric responses depending upon the external magnetic field direction. In addition to the general conventional approach to determine the magnetocaloric effect, we have out line another alternative and most accurate procedure to determine the critical parameters. From the extracted critical parameters from different measurements, along different orientation of the single crystal, magnetic phase diagram also constructed. Study of the magnetic phase diagram may be important from fundamental point view.

Declaration of Competing Interest

The authors declare that they have no known competing financial

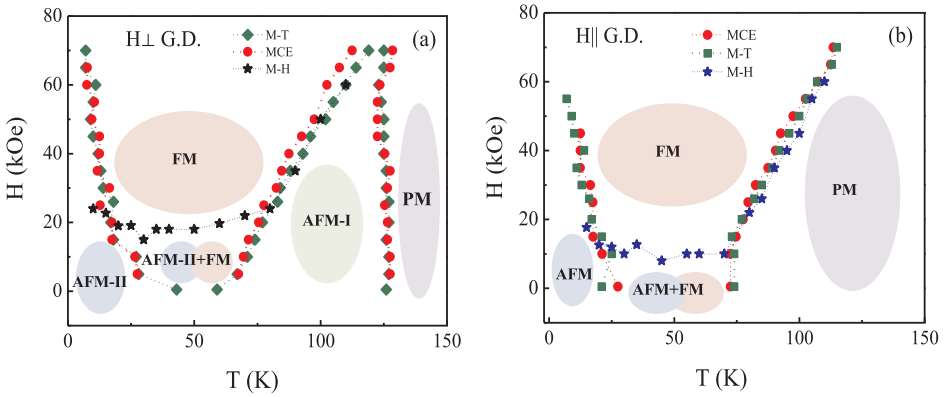

Fig. 11. Magnetic phase diagram of the single crystalline $Sm_{0.5}Ca_{0.25}Sr_{0.25}MnO_3$ compound in different orientation of the sample. Dotted lines through the data points are the guide to the eyes. Shaded regions represent various magnetic states present in the system.

interests or personal relationships that could have appeared to influence the work reported in this paper.

Acknowledgements

The work was supported by Department of Atomic Energy (DAE), Govt. of India. The authors would like to thank A. Paul and S. Banik for their help during sample preparation and magnetization measurements respectively.

References

[1] A.M. Tishin, Y.I. Spichkin, The Magnetocaloric Effect and its Applications, Institute of Physics Publishing, Bristol and Philadelphia, 2003.
[2] K.A. Gschneidner Jr., V.K. Pecharsky, A.O. Tsokol, Rep. Prog. Phys. 68 (2005) 1479.
[3] A.O. Pecharsky, K.A. Gschneidner Jr, V.K. Pecharsky, J. Appl. Phys. 93 (2003) 4722.
[4] J. Liu, T. Gottschall, K.P. Shokov, J.D. Moore, O. Gutfleisch, Nat. Mater. 11 (2012) 620.
[5] H. Zeng, C. Kuang, J. Zhang, Bull. Mater. Sci. 34 (2011) 825.
[6] H. Wada, Y. Tanabe, Appl. Phys. Lett. 79 (2001) 3302.
[7] H. Wada, Y. Tanabe, M. Shiga, H. Sugawara, H. Sato, J. Alloys Compd. 316 (2001) 245.
[8] T. Samanta, I. Das, S. Banerjee, Appl. Phys. Lett. 91 (2007) 152506.
[9] M.H. Phan, S.C. Yu, J. Magn. Magn. Mater. 308 (2007) 325.
[10] A. Rostamnejadi, M. Venkatesan, P. Kameli, H. Salamati, J.M.D. Coey, J. Magn. Magn. Mater. 323 (2011) 2214.
[11] P. Debye, Ann. Phys. 81 (1926) 1154.
[12] W.F. Giauque, J. Am. Chem. Soc. 49 (1927) 1864.
[13] A.J. Millis, P.B. Littlewood, B.I. Shrainman, Phys. Rev. Lett. 74 (1995) 5144.
[14] Q.T. The-Long Phan, P.Q. Tran, P.D.H. Thanh, T.D. Yen, S.C.Yu. Thanh, Solid State Commun. 184 (2014) 40.
[15] M. Dhahri, J. Dhahri, E.K. Hlil, RSC Adv. 8 (2018) 5395.
[16] T. Hashimoto, T. Numasawa, M. Shino, T. Okada, Cryogenics 21 (1981) 647.
[17] J.S. Amaral, V.S. Amaral, Appl. Phys. Lett. 94 (2009) 042506.
[18] M. Winklhofer, R.K. Dumas, K. Liu, J. Appl. Phys. 103 (2008) 07C518.
[19] B.C. Zhao, Y.Q. Ma, W.H. Song, Y.P. Sun, Phys. Lett. A 354 (2006) 472.
[20] T. Paramanik, T. Samanta, R. Ranganathan, I. Das, RSC Adv. 5 (2015) 47860.
[21] K. Das, I. Das, J. Magn. Magn. Mater. 439 (2017) 328.
[22] S. Saha, K. Das, S. Bandyopadhyay, I. Das, J. Magn. Magn. Mater. 432 (2017) 271.
[23] A. Biswas, I. Das, Phys. Rev. B 74 (2016) 172405.
[24] R. M'nassri, Phase Trans. 90 (7) (2016) 687.
[25] H. Zhu, C. Xiao, H. Cheng, F. Grote, X. Zhang, T. Yao, Z. Li, C. Wang, S. Wei, Y. Lei, Yi Xie, Nat. Commun. 5 (2014) 3960.
[26] D.M. Polishchuk, Yu.O.T. Polishchuk, E. Holmgren, A.F. Kravets, A.I. Tovstolytkin, V. Korenivski, Phys. Rev. Mater. 2 (2018) 114402.
[27] F. Cugini, G. Porcari, S. Fabbrici, F. Albertini, M. Solzi, Philos. Trans. R. Soc. A 374 (2016) 20150306.
[28] V.K. Pecharsky, K.A. Gschneidner Jr., Phys. Rev. Lett. 78 (1997) 4494.
[29] H. Wada, Y. Tanabe, Appl. Phys. Lett. 79 (2001) 3302.
[30] H. Wada, K. Taniguchi, Y. Tanabe, Mater. Trans. 43 (2002) 73.
[31] F.X. Hu, B.G. Shen, J.R. Sun, Z.H. Chen, G.H. Rao, X.X. Zhang, Appl. Phys. Lett. 78 (2001) 3675.
[32] A. Planes, L. Manosa, M. Acet, J. Phys.: Condens. Matter. 21 (2009) 233201.
[33] J. Liu, T. Gottschall, K.P. Skokov, J.D. Moore, O. Gutfleisch, Nat. Mater. 11 (2012) 620.
[34] S. Gama, A.A. Coelho, A. de Compos, A.M.G. Carvalho, F.C.G. Gandra, Phys. Rev. Lett. 93 (2004) 237202.
[35] M. Balli, D. Fruchart, D. Gignoux, R. Zach, Appl. Phys. Lett. 95 (2009) 072509.
[36] W. Cui, W. Liu, Z. Zhang, Appl. Phys. Lett. 96 (2010) 222509.
[37] Z. Li, Y. Zhang, K. Xu, T. Yang, C. Jing, H.L. Zhang, Solid State Commun. 203 (2015) 81.
[38] K. Xu, Z. Li, Y.L. Zhang, C. Jing, Phys. Lett. A 379 (2015) 3149.
[39] V. Hardy, A. Maignan, S. Hebert, C. Martin, Phys. Rev. B 67 (2003) 024401.
[40] M. Kataoka, J. Magn. Mater. Mater. 469 (2019) 494.
[41] R. Caballero-Flores, N.S. Bingham, M.H. Phan, M.A. Torija, C. Leighton, V. Franco, A. Conde, T.L. Phan, S.C. Yu, H. Srikanth, J. Phys.: Condens. Matter 26 (2014) 286001.
[42] V.Yu. Ivanov, A.A. Mukhin, A.S. Prokhorov, A.M. Balbashov, Phys. Status Sol. (b) 236 (2003) 445.
[43] M. Respaud, J.M. Broto, H. Rakoto, J. Vanacken, P. Wagner, C. Martin, A. Maignan, B. Raveau, Phys. Rev. B 63 (2001) 144426.
[44] K. Das, J. Magn. Magn. Mater. 458 (2018) 52.
[45] A.I. Abramovich, L.I. Koroleva, A.V. Michurin, J. Phys.: Condens. Matter 14 (2002) L537.
[46] S. Banik, K. Das, I. Das, J. Magn. Magn. Mater. 403 (2016) 36.
[47] D. Shulyatev, S. Karabashev, A. Arsenov, Ya. Mukovskii, J. Crystal Growth 198/199 (1999) 511.
[48] N.G. Bebenin, R.I. Zainullina, V.V. Mashkaustan, V.V. Ustinov, Ya.M. Mukovskii, Phys. Rev. B 69 (2004) 104434.
[49] R. Yang, Y. Sun, X. Ma, Y.K. Tang, Q. Li, Z. Cheng, Phys. Rev. B 73 (2006) 092404.
[50] H.L. Ju, H. Sohn, Solid State Commun. 102 (1997) 463.
[51] P. Vanderbemden, B. Vertruyen, M. Ausloos, B.R. Murias, V. Lovchinov, J. Optoelectron. Adv. Mater. 11 (2009) 115.
[52] J.E. Evetts, M.G. Blamire, N.D. Mathur, S.P. Isaac, B.-S. Teo, L.F. Cohen, J.L.M. Driscoll, Philos. Trans. R. Soc. Lond. A 356 (1998) 1593.
[53] J. Klein, C. Hofener, S. Uhlenbruck, L. Alff, B. Buchner, R. Gross, Europhys. Lett. 47 (3) (1999) 371.
[54] S. Kar, J. Sarkar, B. Ghosh, A.K. Raychaudhuri, J. Nano Nanotechnol. 7 (2007) 2051.
[55] A. Biswas, T. Samanta, S. Banerjee, I. Das, Appl. Phys. Lett. 92 (2008) 012502.
[56] A. Arulraj, P.N. Santhosh, R.S. Gopalan, A. Guha, A.K. Raychaudhuri, N. Kumar, C.N.R. Rao, J. Phys.: Condens. Matter 10 (1998) 8497.
[57] Y. Tokura, Y. Tomioka, J. Magn. Magn. Mater. 200 (1999) 1.
[58] Y. Tokura, Rep. Prog. Phys. 69 (2006) 797.
[59] Y. Tomioka, H. Hiraka, Y. Endoh, Y. Tokura, Phys. Rev. B 74 (2006) 104420.
[60] S. Zhou, Y. Guo, J. Zhao, L. He, L. Shi, J. Phys. Chem. C 115 (2011) 1535.
[61] S. Banik, K. Das, T. Paramanik, N.P. Lalla, B. Satpati, K. Pradhan, I. Das, NPG Asia Mater. 10 (2018) 923.
[62] T. Paramanik, K. Das, T. Samanta, I. Das, J. Magn. Magn. Mater. 381 (2015) 168.
[63] A. Beiranvand, J. Tikkanen, H. Huhtinen, P. Paturi, J. Alloys Compd. 720 (2017) 126.
[64] S. Zhou, Y. Guo, C. Wang, L. He, J. Zhao, L. Shi, Dalton Trans. 41 (2012) 7109.
[65] J. Hejtmanek, Z. Jirak, J. Sebek, A. Strejc, J. Appl. Phys. 89 (2001) 7413.
[66] Z. Shu, J. Dong, D.Y. Xing, Phys. Rev. B 63 (2001) 224409.
[67] A.M. Tishin, J. Magn. Magn. Mater. 184 (1998) 62.
[68] F. Perez, T. Werner, J. Wosnitza, H.V. Lohneysen, Phys. Rev. B 58 (1998) 9316.
[69] R. Bugel, A. Faibt, H.V. Lohneysen, J. Wosnitza, U. Schotte, Phys. Rev. B 65 (2001) 052402.
[70] D.M. Radheep, P. Sarkar, S. Arumugam, R. Suryanarayanan, P. Mandal, J. Magn. Magn. Mater. 365 (2014) 51.
[71] J. Dho, N.H. Hur, Phys. Rev. B 67 (2003) 214414.
[72] D.S. Rana, R. Nirmala, S.K. Malik, Europhys. Lett. 70 (2005) 376.
[73] V. Hardy, S. Hebert, A. Maignan, C. Martin, M. Hervieu, B. Raveau, J. Magn. Magn. Mater. 264 (2003) 183.
[74] V. Hardy, S. Majumdar, S.J. Crowe, M.R. Less, D. McK Paul, L. Herve, A. Maignan, S. Hebert, C. Martin, C. Yaicle, M. Hervieu, B. Raveau, Phys. Rev. B 69 (2004) 020407(R).
[75] A. Rostamnejadi, M. Venkatesan, P. Kameli, H. Salamati, J.M.D. Coey, J. Magn. Magn. Mater. 323 (2011) 2214.
[76] R. M'nassri, Bull. Mater. Sci. 39 (2016) 551.